Energy 66 (2014) 401–412

Contents lists available at ScienceDirect

Energy

journal homepage: www.elsevier.com/locate/energy

Software method for harmonic content evaluation of grid connected converters from distributed power generation systems

L. Barote*, C. Marinescu

Transilvania University of Brasov, Electrical Engineering and Applied Physics Department, 1st Politehnicii Street, 500024 Brasov, Romania

ARTICLE INFO

Article history:
Received 13 May 2013
Received in revised form
16 December 2013
Accepted 21 December 2013
Available online 17 January 2014

Keywords:
Grid converter control
Current controller
Harmonic compensator
Power quality

ABSTRACT

This paper is deals with the implementation of a software control method for harmonic content evaluation in the *dq* synchronous rotating reference frame for grid side VSIs (Voltage Source Inverters) used in DPGS (distributed power generation systems) applications. In order to verify the performance of the proposed approach, in experiments a DC voltage source (playing the role of a generic renewable energy source) is connected to the grid using a two-level inverter. Additionally, the control structure of the grid side converter is presented the possibility of low order harmonics compensation is also discussed. A comparative study in terms of current harmonic distortion between two different proportional gain values of the PI controller running in steady state condition is made, through simulations and experiments. The comparative study is performed to demonstrate the stability and effectiveness of the PI control algorithm across a wide range of operating conditions with the software method. The analyzed structure was simulated using Simulink software and then implemented and tested at laboratory level using a dSPACE setup. The experimental and simulation results confirm that the proposed software control method achieves good current tracking, thus satisfying grid-connection harmonics standards.

© 2014 Elsevier Ltd. All rights reserved.

I. Introduction

Nowadays fossil fuels are the main energy supplier for the worldwide economy. However, as they are depleting and cause significant environmental problems, the focus is moving towards on alternative resources for power generation. RES (renewable energy sources) like wind, sun and small and micro hydro are seen as a reliable alternative to the traditional energy sources. DPGS (distributed power generation systems) based on renewable energy resources experience a constant growth. The majorities of renewable energy systems are connected to the utility network by power electronics, and are spread along the power system.

Consequently, grid interconnection requirements are evolving towards distributed generators which are able to accommodate control algorithms that enable a better control of generated power and the ability to contribute to power system stability if necessary [1,2]. Different control strategies and configurations of hybrid distributed generation systems are presented in Ref. [3] and a literature review of grid-connected versus stand-alone energy systems can be found in Refs. [4,5].

The increased interest in renewable energy production coupled with higher and higher demand from the energy distribution companies, with respect to grid energy injection and grid support in case of a failure, raises new challenges in terms of control for RES systems [6]. A general block diagram of a DPGS is shown in Fig. 1. The generated power can be delivered to the local loads or can be injected into the utility network, depending where the generation system is connected. In our configuration the latter case is considered.

The main aspects investigated in this paper are the control part of a power converter connected to the grid by means of a passive filter and an adequate harmonic compensation technique. In the literature, different power converter topologies are used to interface DPGS with the utility network [7–11]. In this work, the investigation is limited to the control of a three phase PWM (pulse width modulated) two level VSI (voltage source inverter), the most used power electronic interface for RES [12]. In order to accommodate a wide range of DPGS, the input power sources are not considered, the inverter being powered by a DC power source.

A synchronous rotating *dq* frame PI current controller was chosen to control the VSI. A description of the advantages and disadvantages of the *dq*-PI current controller is presented in Refs. [13,14]. The quality of the injected current is influenced by the current control strategy.

* Corresponding author.
E-mail address: luminita.barote@unitbv.ro (L. Barote).

0360-5442/$ – see front matter © 2014 Elsevier Ltd. All rights reserved.
http://dx.doi.org/10.1016/j.energy.2013.12.050

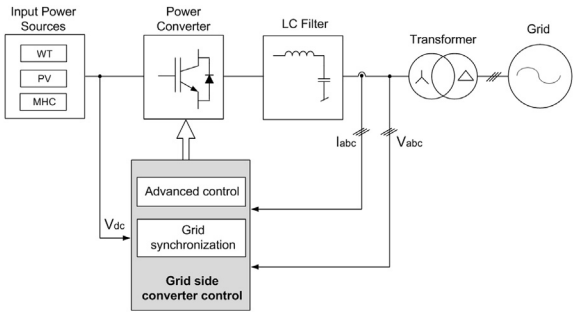

Fig. 1. Block diagram of the analyzed grid connected topology.

Traditionally, the inverter output current is improved by tuning the controllers while monitoring the low order harmonics. As a trade-off between a good noise rejection and good dynamics for the analyzed structure, the tuned parameters of the PI controller used in the simulation and experiments are set as follows: the integrator gain was set to $K_i = 1000$ while two different values ($K_p = 10$ and $K_p = 20$) were chosen for the proportional gain value, which determines the bandwidth and stability phase margin [15–17]. The controller gains were determined by trial and error method and the values are not changed when the controller is transformed in different reference frames [18]. A comparative study between these two values is presented in the simulation and experimental section. By adding a HC (Harmonic Compensator) to the current controller, a good harmonics rejection is obtained in both analyzed cases. A PLL (phase locked loop) is employed in order to detect the grid phase angle θ and the grid frequency.

The proposed software control method has the capability of providing active and reactive powers and as well harmonic currents with a fast dynamic response. In the different simulation and experimental results of the analyzed cases (without and with HC) have been completed in order to achieve controller effectiveness and a reduced THD (total harmonic distortion). The results prove the high performance of this control strategy in DPGS applications in comparison with other existing strategies. Another advantage is that the proposed control method can be used for different types of distributed generation resources as power quality improvement devices in a power distribution network.

The reminder of this paper is organized as follows: in Section 2 the configuration of the grid connected system with the control methods is presented. Section 3 describes the simulation and experimental results while conclusions are provided in Section 4.

2. Controller configuration for grid connected system

The configuration of the analyzed grid connected inverter is shown in Fig. 1. A DC power supply is considered as input power sources; a VSI with PI current controller and HC (Harmonic Compensator), a synchronization technique, a LCL (inductive–capacitive–inductive) filter, a delta transformer connection and the utility grid complete the topology.

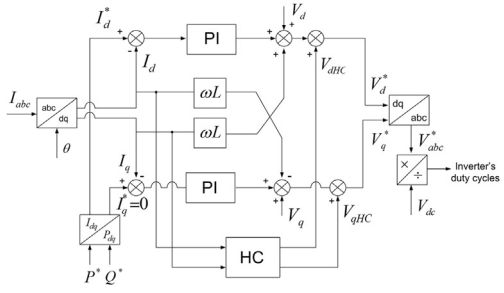

Fig. 2. The *dq* current control based on PI controller with HC.

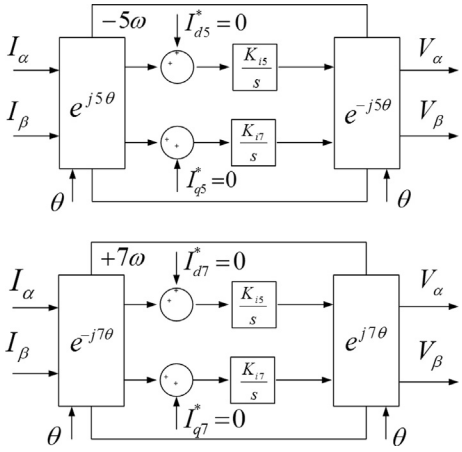

Fig. 3. The HC diagram for PI controllers.

Fig. 2 shows the structure of the grid side converter control circuit based on PI current controllers in *dq* frame control involving cross coupling and feed forward of the grid voltages. By using the Park's transformation, the three phase currents and voltages are transformed from the *abc* frame into the *dq* frame.

The i_q current component determines the reactive power value while the i_d decides the active power flow. Thus the active and reactive power can be controlled independently.

Beside the use of PI controllers for current regulation, as Fig. 2 illustrates, cross-coupling terms and the grid voltage feed-forward may be necessary in order to obtain best results [19].

The current controller input is the error between the measured and the reference grid currents. The current controller output is the reference grid voltage, which divided by the DC source voltage gives the inverter duty cycle. A HC is applied in synchronous reference frames, where the currents are DC quantities, thus eliminating the steady-state error, in order to obtain an improved power quality for the studied configuration.

In the case of DPGS, high dynamics and harmonics compensation, especially low order harmonics, are required. The compensation capability of the low order harmonics in the case of PI controllers is very poor without HC, standing as a major drawback when using it in grid connected systems. For this reason it is necessary to use a HC technique.

As the most important harmonics in the current spectrum are usual the 5th and 7th (see Fig. 14), in this paper the HC is designed to compensate these two selected harmonics. As shown in Fig. 3, the two controllers should be implemented in two frames rotating at −5ω and +7ω. Two transformation modules are necessary to transfer the αβ stationary quadrature system into a *dq* synchronous rotating frame and vice versa. Noticeable is in this case the complexity of the control algorithm, compared with the structure implemented in stationary reference frame [15,20].

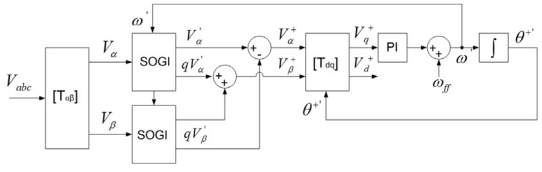

Fig. 4. Block diagram of the three-phase DSOGI-PLL.

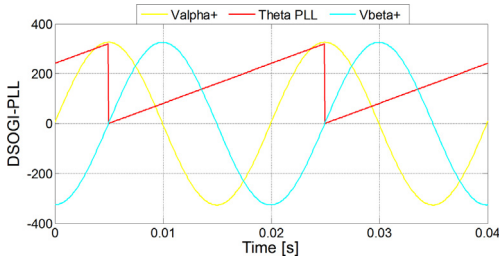

Fig. 5. Grid phase angle.

In order to synchronize the injected grid current with the grid voltage, a PLL block is used. A DSOGI (Dual Second Order Generalized Integrator) is employed in the QSG (Quadrature-Signals Generator) to obtain two couples of orthogonal and cleaned signals. Practically the grid disturbances are filtered before entering in the PLL scheme [15,21].

The structure of this DSOGI-based PLL (DSOGI-PLL) is presented in Fig. 4, where the positive-sequence voltage vector is translated from the $\alpha\beta$ stationary reference frame to the dq rotating reference frame by means of Park's transformation.

In the system shown in Fig. 4, the feedback loop regulating the q component to zero is controlling the angular position of the dq reference frame and estimating the grid frequency. The PI controller output and the feed forward frequency ω_{ff} are modulated and give the phase angle, θ. A settling time of 10 ms was used in order to get a satisfied high bandwidth of the PLL controller. The grid phase angle with the voltages ($V_\alpha^+ V_\beta^+$) is depicted in Fig. 5.

The active and reactive powers flowing from an inverter to the grid can be described and expressed as in Fig. 6. The P/Q droop control method [22,23] has the ability to change the active and reactive power references according to the system requirements. Therefore, in the studied configuration, the reference active power values are set to $P^* = 500$; 1000; 1500; 2000 W and $Q^* = 0$ var. The nominal power of the considered grid side inverter is 2.2 kVA.

Fig. 7 presents the software method for harmonic content evaluation of grid connected converters from a distributed generation system based on renewable energy sources. The method consists of an active and reactive power calculation block (droop control – see Fig. 6) and a voltage–current (VI) control structure, with a PI controller (see Fig. 2) and a harmonic compensator (see Fig. 3), both implemented in a dq synchronous reference frame. The VI control structure is presented in Fig. 8. The output voltage of the controller from the VI control block is multiplexed; the resulting value provides voltage signals which enter to the PWM generator to yield output modulated signals for the grid converter. The proportional-integral coefficients can be fixed/modified according the system parameters.

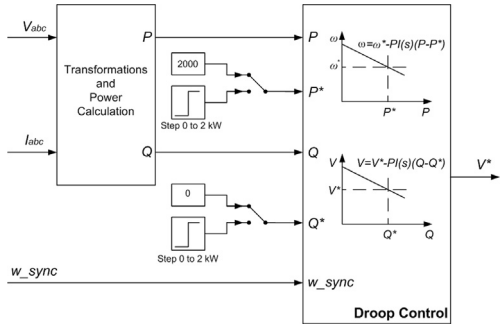

Fig. 6. The P/Q droop implementation within the studied configuration.

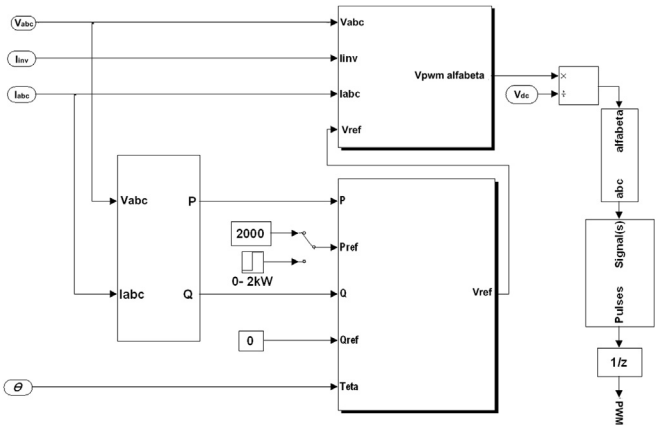

Fig. 7. Software method for harmonic content evaluation of grid connected converters.

3. Simulation and experimental results

The proposed system was modeled and simulated using the Matlab/Simulink environment, Fig. 9 showing the block diagram. The system's parameters can be set according to the used experimental setup to validate the simulation results.

The PWM inverter switching frequency was set to 10 kHz, while an LCL filter is placed between the inverter and the grid.

The voltage–current control of the grid side inverter was implemented in a dSPACE platform and its performance evaluated. The setup block diagram is presented in Fig. 10 and consists of a three-phase inverter with a rated power of 2.2 kVA, two series connected DC power supplies (3 kW, 330 V), an LCL filter (see Table 1), LEM boxes for the measurement of V_{dc}, I_{abc} and V_{abc}, a three-phase transformer (5 kVA) and a dSPACE system. The parameters of the system are presented in Table 1.

The implemented LCL filter consists of three reactors with resistance R_I and inductance L_I on the converter side and three capacitors C_F; a further branch of the filter, represented as three

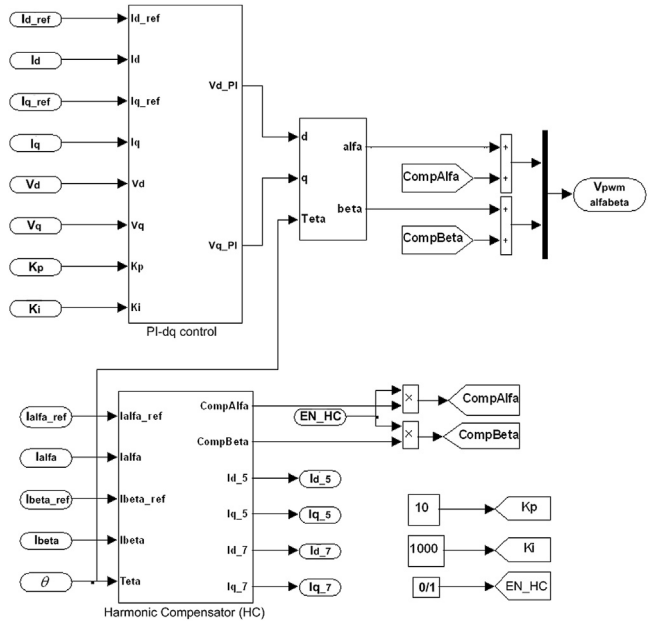

Fig. 8. Control structure implemented for grid converter with PI-dq controllers with HC.

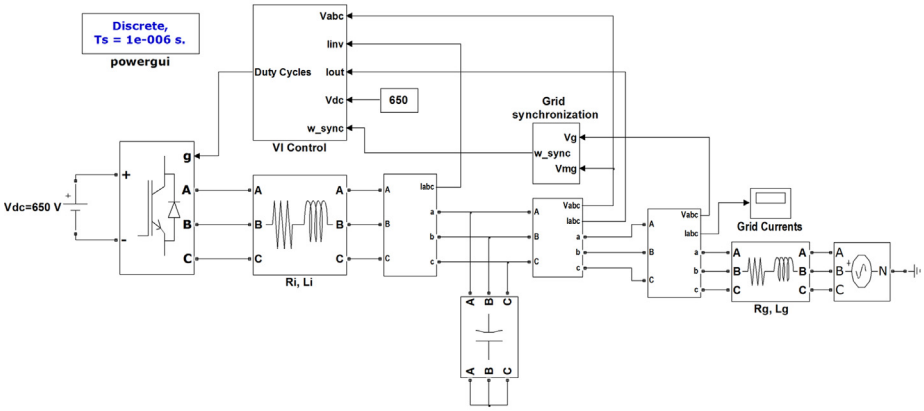

Fig. 9. Simulink block diagram.

reactors with resistance R_G and inductance L_G, comes from taking in account the impedance of the transformer adopted for the connection to the grid and the grid impedance. The filter's role is to reduce high frequency current ripple injected by the inverter [24].

A control system with the proposed software method was developed in Matlab/Simulink and then automatically processed and implemented in the DS1103 PPC card. A GUI (Graphical User Interface) (see Fig. 11) has been build using the Control Desk software in order to allow a real time control and evaluation of the system.

The GUI can be used to control inputs such us: start/stop of the system; active and reactive power references and current control methods. It can also be used to view different outputs such us: measured three phase grid currents and voltages; measured DC voltage; measured active and reactive power; the phase angle provided by the PLL, etc. Furthermore, different experimental cases can be tested, like a step or stairs in the active power reference to confirm the good implementation of the analyzed current control method.

Simulation and experimental results are presented to validate the effectiveness of the control strategies used. The laboratory tests follow the same line as the ones carried out in simulation.

The experimental set-up can be generalized and other controllers, parameters and different control inputs/outputs can be added. In our case, a control system was developed in Matlab/Simulink and the Graphical User Interface (see Fig. 11) has been build using the Control Desk software in order to allow a real time control and evaluation of the system. The software method was created for tested the PI controller at different active and reactive power, with the same parameters.

In order to validate a proper system operation with proposed software control method, the following simulations and experiments were carried out.

Case 1: Different variations in the active and reactive power references for the PI controller parameters ($K_p = 10$, $K_i = 1000$, $K_{i5,7} = 150$) without and with HC;

Case 2: Different variations in the active and reactive power references of the PI controller parameters ($K_p = 20$, $K_i = 1000$, $K_{i5,7} = 150$) without and with HC;

Case 3: Comparative analysis between Case 1 and Case 2 is performed.

To test the dynamic performance of the grid-connected system, two more experimental cases have been chosen to validate the implementation of the current controller with proposed software method.

Case 4: Step change in the active power reference of the PI controller parameters ($K_p = 10$, $K_i = 1000$, $K_{i5,7} = 150$) without and with HC;

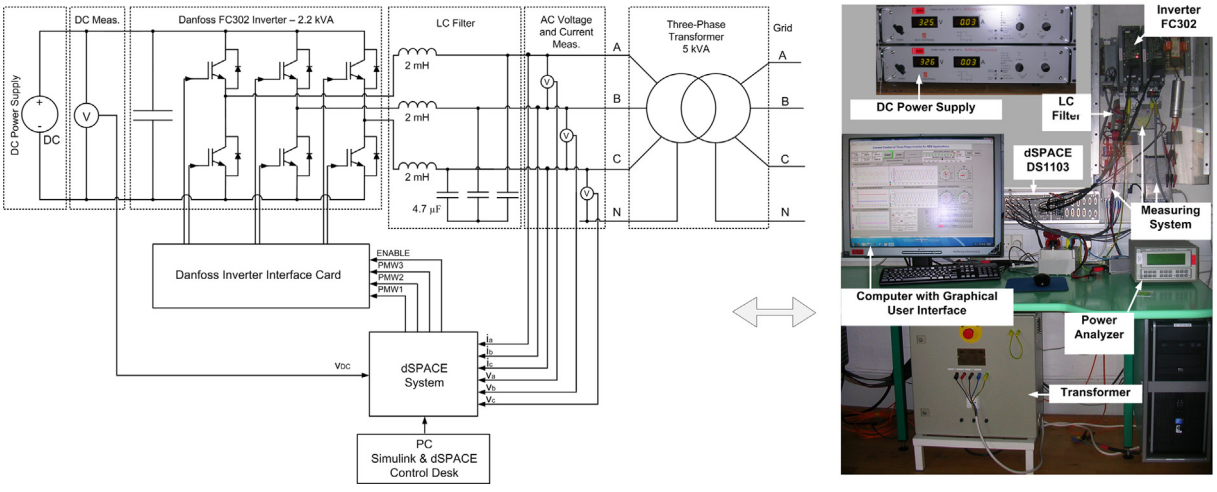

Fig. 10. Experimental setup.

Table 1
The hardware setup.

Parameter	Value
Grid voltage (line–line rms)	380 V
Grid frequency	50 Hz
Inverter-side inductance	$L_I = 6.9\ mH$
Inverter-side resistance	$R_I = 0.1\ \Omega$
Grid side inductance (transformer inductance)	L_G=2 mH
Grid side resistance	$R_G = 1.4\ \Omega$
Filter capacitance	$C_F = 4.7\ \mu F$
Switching frequency	$f_s = 10$ kHz

Case 5: Stairs change in the active power reference of the PI controller parameters ($K_p = 10$, $K_i = 1000$, $K_{i5,7} = 150$) without and with HC.

3.1. Case 1: different variations in the active and reactive power references for the PI controller parameters ($K_p = 10$, $K_i = 1000$, $K_{i5,7} = 150$) without and with HC

In the first part, the measurements were performed for four different reference values of the active power (starting with 500 W–2000 W steps), without and with HC, while the reactive power reference was set to 0. The control parameters variation depending on the input power variation is evaluated. Fig. 12 shows that the i_d and i_q/P and Q measured signals are tracking their references very well.

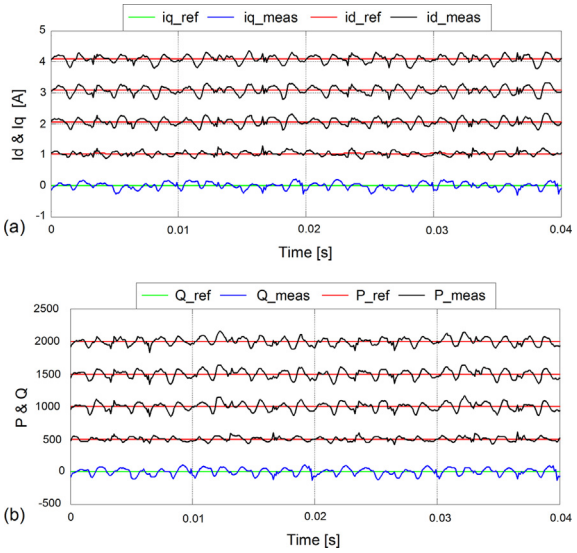

Fig. 12. (a) I_d and I_q reference and measured currents; (b) P and Q reference and measured powers.

Fig. 13 shows the grid injected current for phase A (I_a) in the case of control with PI controller without HC in both, simulation (Fig. 13a) and experimental (Fig. 13b) cases.

Total harmonic distortion (THD) is an important index widely used to describe power quality issues in transmission and

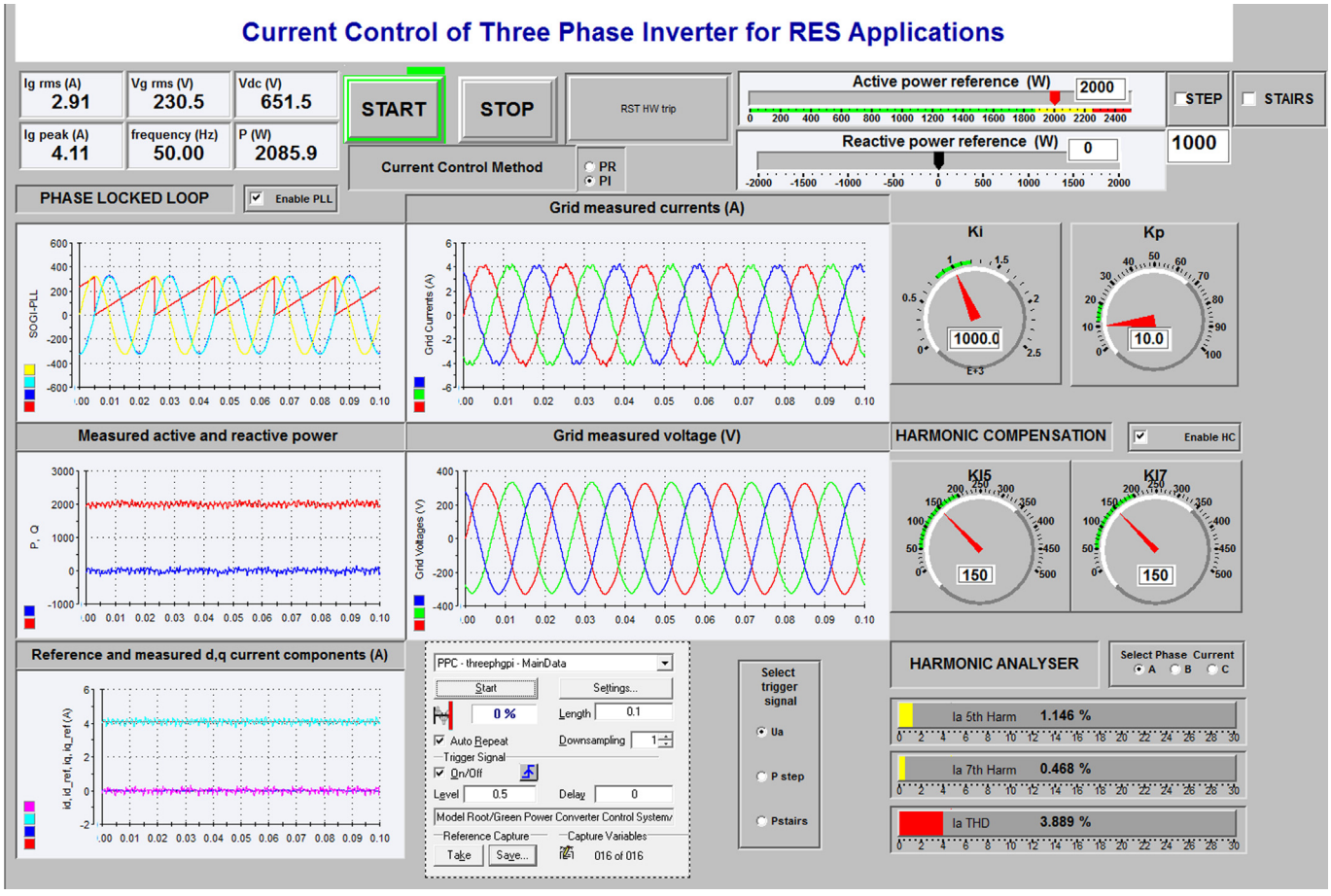

Fig. 11. Control desk GUI.

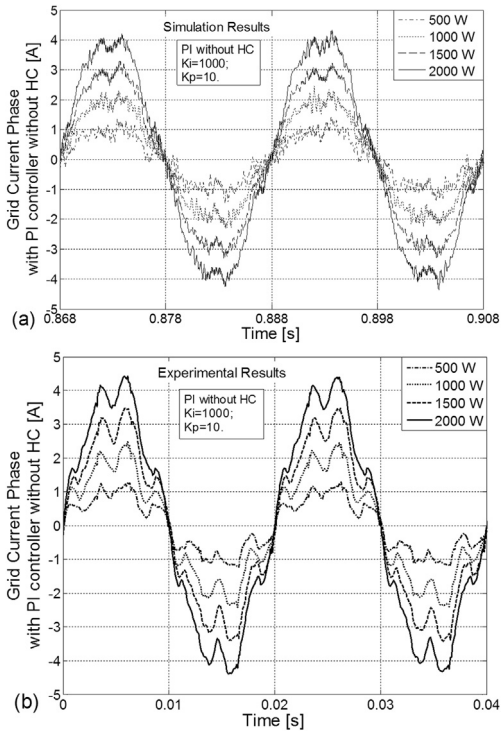

Fig. 13. Grid current (I_a) in the case of PI controller without HC: a) Simulation results; b) Experimental results.

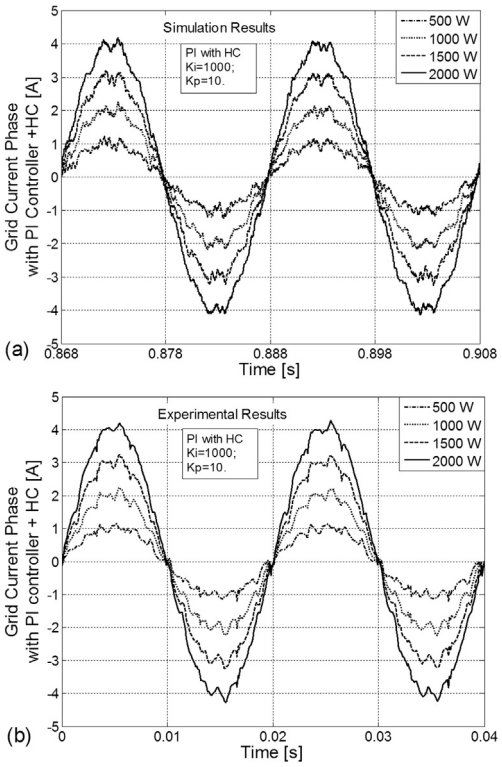

Fig. 15. Grid current (I_a) in the case of PI controller with HC: a) Simulation results; b) Experimental results.

distribution systems [25]. The THD of the grid current containing the 5th and 7th harmonics were presented numerically using the control desk graphical interface (see Fig. 11). However, for the graphic representation of the harmonic spectrum for both cases, measured grid currents were implemented in Matlab and with the discrete powergui, the Fast Fourier Transform (FFT) analysis was made for each active power value.

The THD spectrum of the grid currents in the simulation and experimental cases was evaluated starting at 0.888 s and 0.02 s for 1 cycle in all considered cases. The results of using a $K_p = 10$ gain for PI controller without HC, can be seen in Fig. 14.

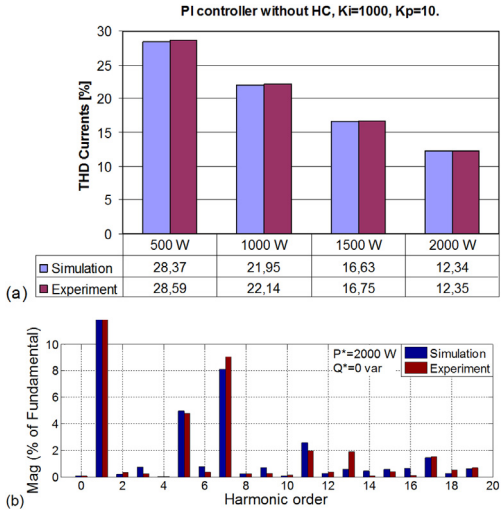

Fig. 14. THD representation of the grid current phase without HC in both simulation and experimental cases for: (a) different values of active power; (b) $P^* = 2000$ W (harmonics spectrum).

It can be seen that the used current control method provides a THD that is higher than the limit imposed by the standard IEEE 1547.2 [26]. As such, the power quality delivered to the network must be improved by using the HC technique in order to keep the THD below the requested 5%.

After the HC implementation, the THD level decreases and a good power quality is obtained. The results for grid currents together with the harmonic spectrum at different active power reference values are presented in Figs. 15 and 16.

As it can be seen in Fig. 12a, at $P^* = 2000$ W, the PI control technique without compensation provides a THD of 12.35%

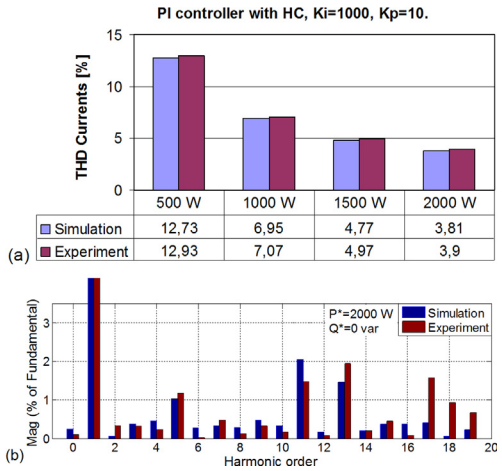

Fig. 16. THD representation of the grid current phase with HC in both simulation and experimental cases for: (a) different values of active power; (b) $P^* = 2000$ W (harmonics spectrum).

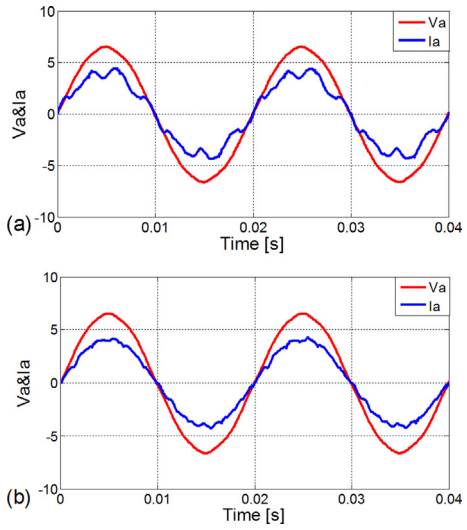

Fig. 17. Experimental results for grid voltage and current for $K_p = 10$, $K_i = 1000$ in the case of: a) PI without HC; b) PI with HC.

(experiment results) and after the HC implementation, the THD level decreases to 3.9% (Fig. 16a) and a good power quality is obtained.

In order to check if the unity power factor is achieved, in Fig. 17, the A phase grid voltage ($V_A/50$) is plotted together with the phase grid current (I_a) for the same case as presented before. It can be noticed that the grid current and voltage are in phase, for the reactive power reference fixed to 0.

In the second part, the measurements were performed at two different reference values of reactive power (1000 var and −1000 var) without and with HC and the active power reference set to 2000 W.

In order to test if the current controller from the q axis works in a proper manner, the reactive power reference initially was set at 2 A ($\approx Q^* = 1000$ var). It can be seen in Fig. 18a how the measured q component of the current is following its reference, thus proving the effectiveness of the controllers. Therefore, the active and reactive power delivered to the grid can be independently

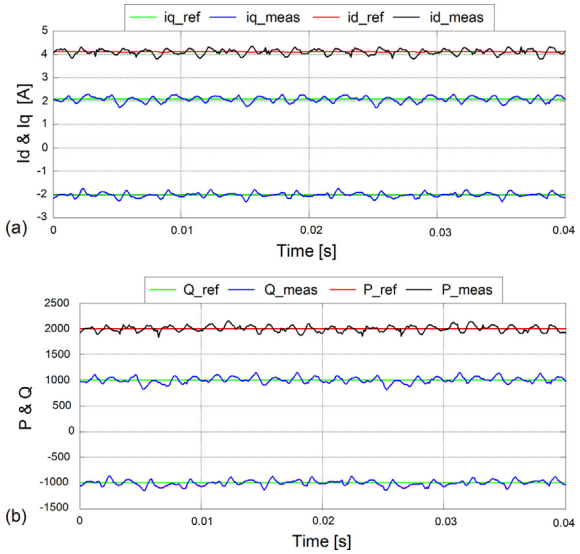

Fig. 18. (a) I_d and I_q reference and measured currents; (b) P and Q reference and measured powers.

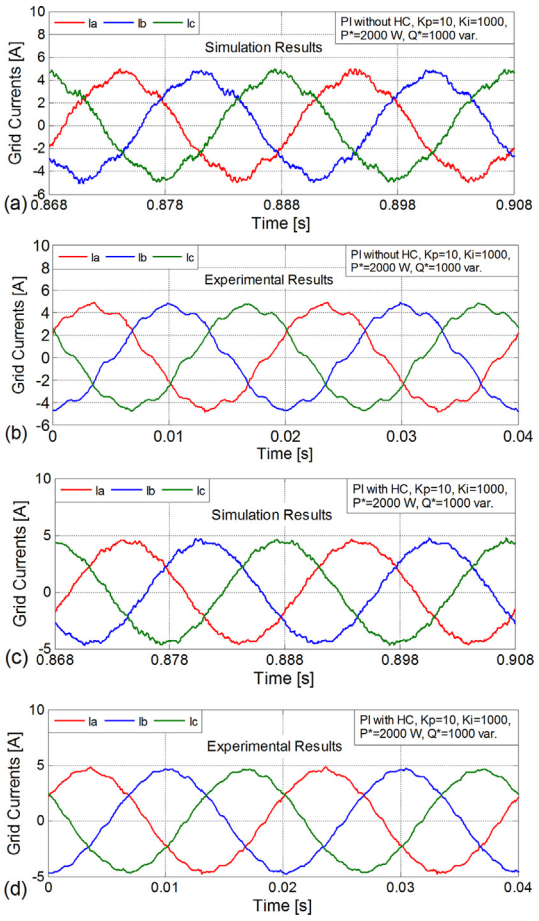

Fig. 19. Grid currents in the case of PI controller without/with HC for $P^* = 2000$ W and $Q^* = 1000$ in both simulation and experimental cases.

controlled. Fig. 18 shows the reference and measured dq currents/P, Q powers for this case.

Fig. 19 shows the measured grid currents for $P^* = 2000$ W and $Q^* = 1000$ var in both simulation and experimental results, without and with HC. In this case, the VSI is able to inject the desired reactive power into the grid. The THD harmonic spectrum of the grid current without and with HC is presented in Fig. 20. As can be seen, better results are obtained compared with the previously case

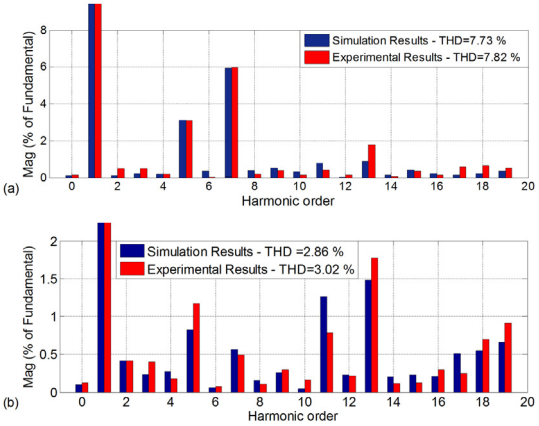

Fig. 20. THD harmonic spectrum of the grid current (I_a) in both simulation and experimental cases for. (a) PI without HC; (b) PI with HC.

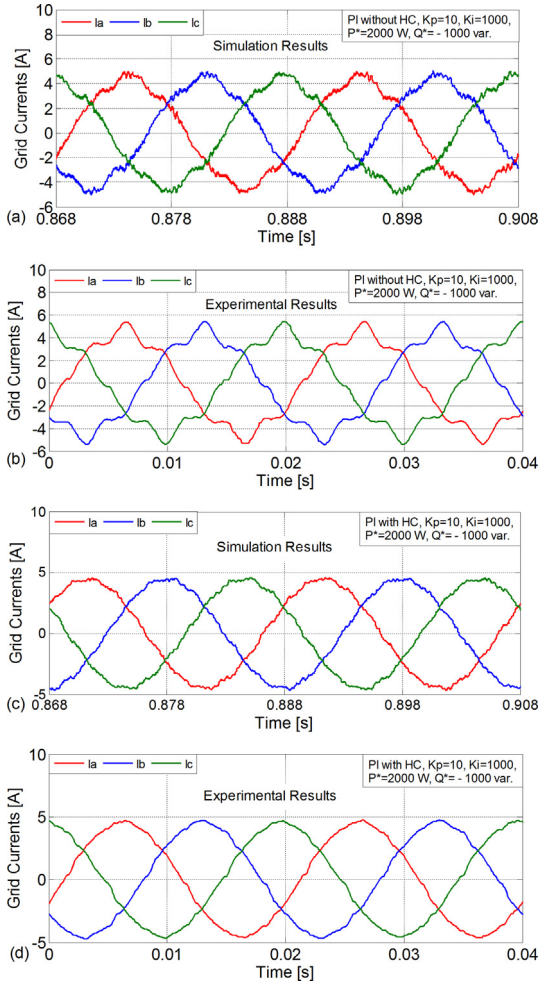

Fig. 21. Grid currents in the case of PI controller without/with HC for $P^* = 2000$ W and $Q^* = -1000$ in both simulation and experimental cases.

($P^* = 2000$ W, $Q^* = 0$ var), meaning that the positive reactive reference power has a good influence on the THD grid currents (the filtering effect of the inductive elements is displayed).

To test again the performance of the analyzed grid connected system with the proposed software control method, the current

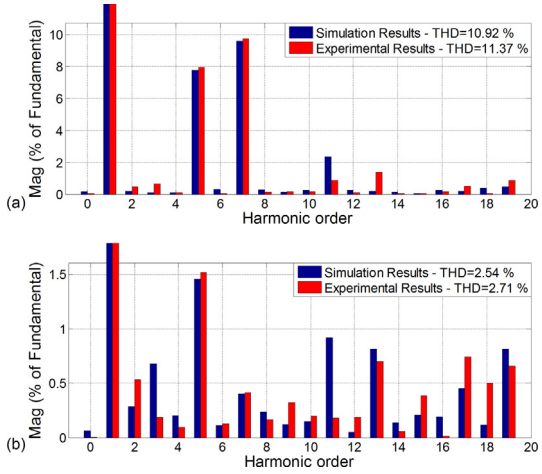

Fig. 22. THD harmonic spectrum of the grid current phase (I_a) in both simulation and experimental cases for: (a) PI without HC; (b) PI with HC.

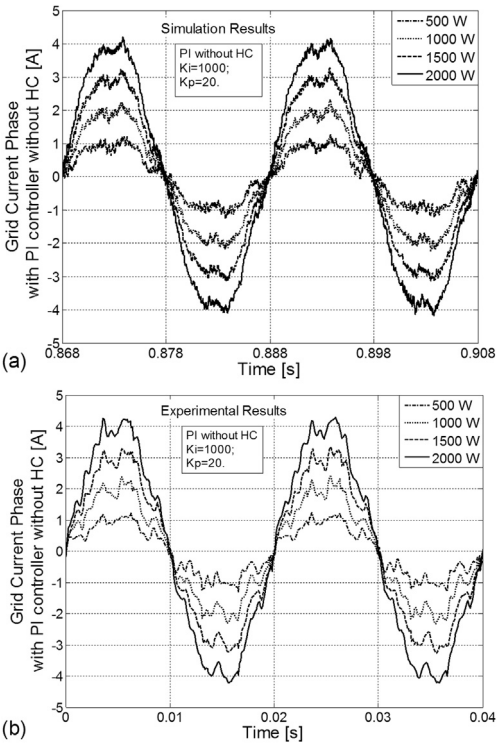

Fig. 23. Grid current (I_a) in the case of PI controller without HC: a) Simulation results; b) Experimental results.

reference is changed to −2 A ($\approx Q^* = -1000$ var – see Fig. 18), while keeping $P^* = 2000$ W. Changing the q-axis reference current will lead to changes in the three-phase currents injected by the converter into the grid. The VSI capability to absorb 1000 var of reactive power is shown in Fig. 16b. Fig. 21 shows the injected currents into the grid, while the corresponding recorded THD for phase A (I_a) is shown in Fig. 22.

Comparing the results of Fig. 20 with those of Fig. 22, it can be seen that a better energy quality is obtained for $P^* = 2000$ W/$Q^* = 1000$ var, in the case of PI controller without HC (see Fig. 20a) and for $P^* = 2000$ W/$Q^* = -1000$ var, after HC implementation (see Fig. 22b). Note that, the best results in terms of THD were obtained

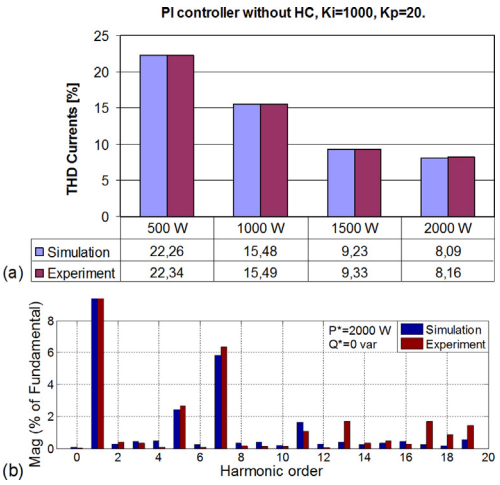

Fig. 24. THD representation of the grid current (I_a) without HC in both simulation and experimental cases for: (a) different values of active power; (b) $P^* = 2000$ W (harmonics level).

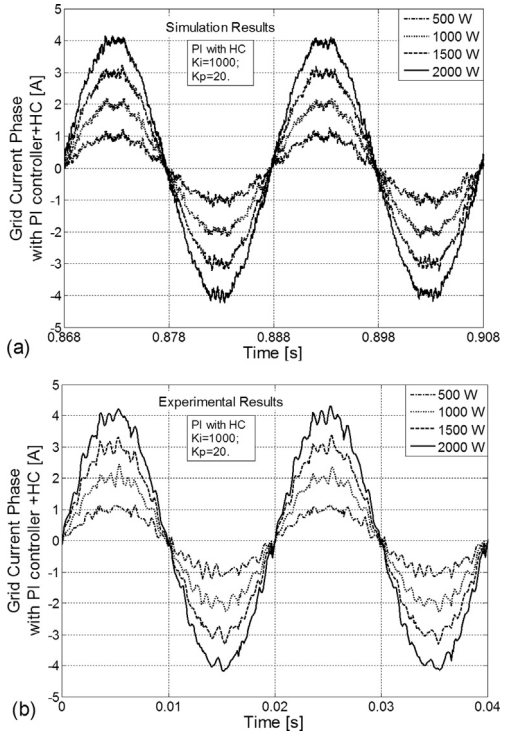

Fig. 25. Grid current (I_a) in the case of PI controller with HC ($K_i = 1000$, $K_p = 20$): a) Simulation results; b) Experimental results.

for all cases, in both simulation (2.54%) and experimental results (2.71%) using the approach.

3.2. Case 2: different variations in the active and reactive power references for PI controller parameters ($K_p = 20$, $K_i = 1000$, $K_{i5,7} = 150$), without and with HC

In the second case, simulation and experimental conditions remain the same as in the first case, except the proportional gain of the PI controller, which was set to $K_p = 20$. For a comparative analysis, the simulations and measurements were performed for the same values of active power, without and with HC. The grid current in the case of the PI controller without HC is presented in Fig. 23. It can be seen that the value of grid current changes with the increase in the active power, starting from approx. 1 A at 500 W until approximately 4 A at 2000 W.

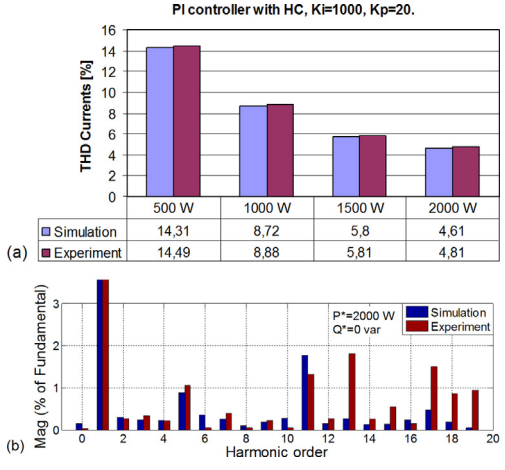

Fig. 26. THD representation of the grid current (I_a) with HC in both simulation and experimental cases for: (a) different values of active power; (b) $P^* = 2000$ W (harmonics spectrum).

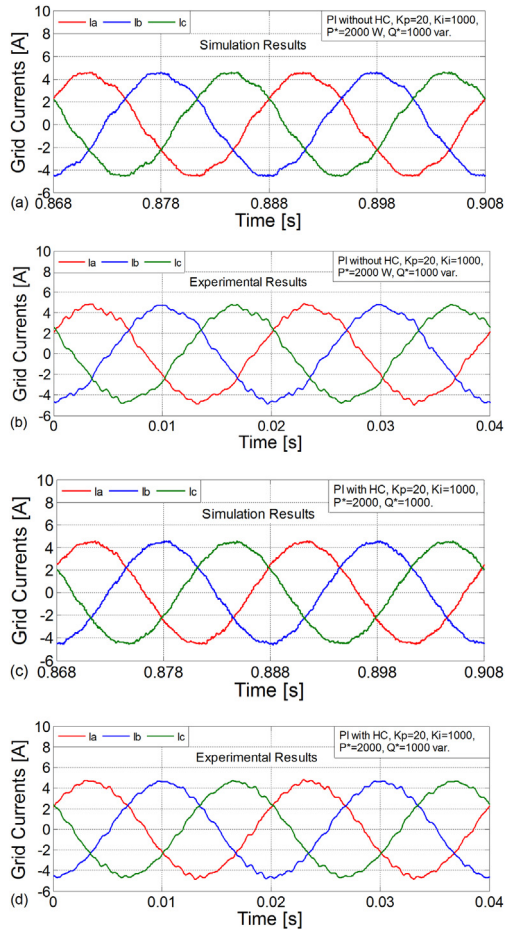

Fig. 27. Grid currents in the case of PI controller without/with HC for $P^* = 2000$ W and $Q^* = 1000$ in both simulation and experimental cases.

As results from Fig. 24a, grid currents THD decreases when the reference power reaches the rated power of the VSI. A detailed harmonic order representation for 2000 W is presented in Fig. 24b (Fig. 25).

As can be seen in Fig. 24, the THD level is lower than the values from Fig. 15, without HC implementation, which means that in this

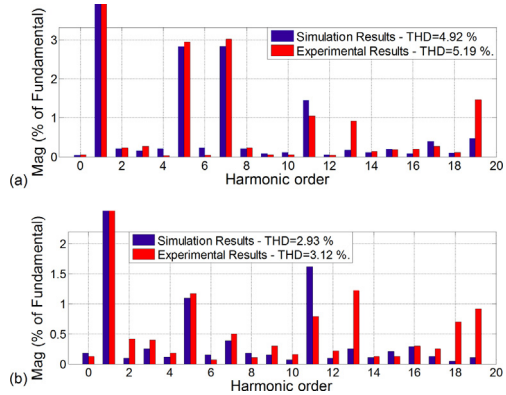

Fig. 28. THD harmonic spectrum of the grid current (I_a) in both simulation and experimental cases for: (a) PI without HC; (b) PI with HC.

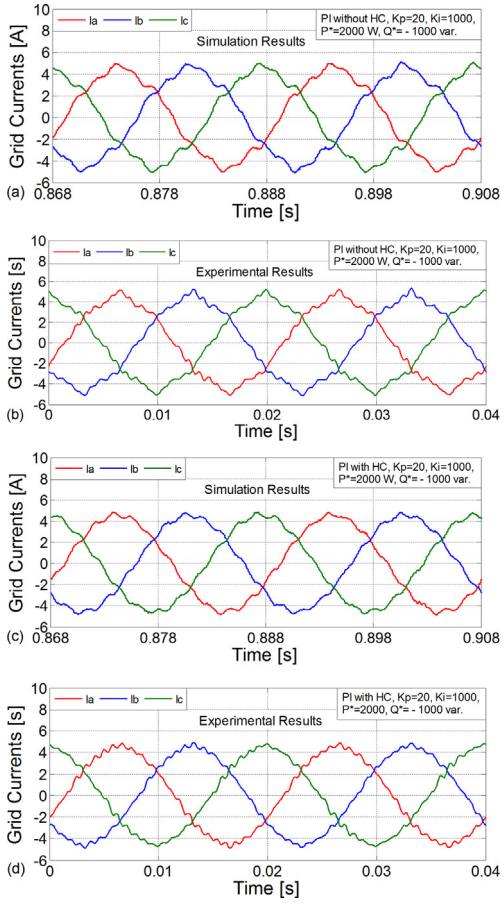

Fig. 29. Grid currents in the case of PI controller without/with HC for $P^* = 2000$ W and $Q^* = -1000$ in both simulation and experimental cases.

case, increasing the PI proportional gain leads to the decrease of THD. After the HC implementation, the current THD is drastically reduced. In Fig. 26 one can observe that the THD is within the limits imposed by the standard [26] at $P^* = 2000$ W for $K_p = 20$.

As in the first case, the goal was to test the influence of reactive power on the THD current injected into the grid for $K_p = 20$. The results obtained for simulated and measured grid currents with harmonics level at $P^* = 2000$ W, $Q^* = 1000$ var, are presented in Figs. 27 and 28.

Even if the grid currents THD value for the analyzed case is lower for $K_p = 20$ than for $K_p = 10$ without HC implementation,

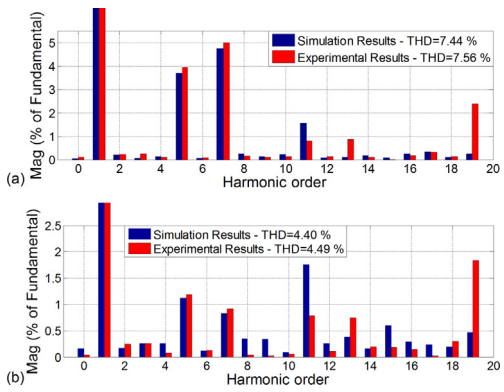

Fig. 30. THD harmonic spectrum of the grid current (I_a) in both simulation and experimental cases for $K_p = 20$: (a) PI without HC; (b) PI with HC.

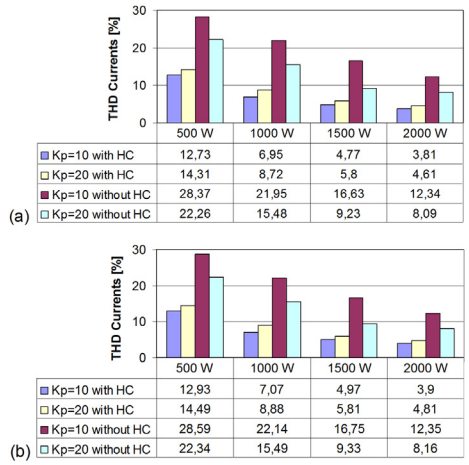

Fig. 31. Comparative analysis between different values of active power, with/without HC: (a) Simulation results; (b) Experimental results.

nevertheless the values are very close to the limit imposed by the standards and is recommended to include a HC in the control structure. After the HC implementation, good performance is obtained. The THD harmonic spectrum of the grid current (I_a) in the simulation and experimental cases, without and with HC, is presented in Fig. 28.

Fig. 29 shows the injected currents into the grid when the reactive power reference is changed to −1000 var, while the corresponding recorded THD for phase A (I_a) is shown in Fig. 30. Comparing the results of Fig. 28 with those of Fig. 30, it can be seen that a better energy quality is obtained for $P^* = 2000$ W, $Q^* = 1000$ var in both simulation and experimental cases, without and with HC. In this case, we can see much better the inductive filter character on the grid currents, compared to the capacitive one.

3.3. Case 3: comparative analyses

To better visualize the cases subject to evaluation, in Figs. 31 and 32 a comparative analysis between the above cases was made. In Fig. 31, the comparative study was performed at four different

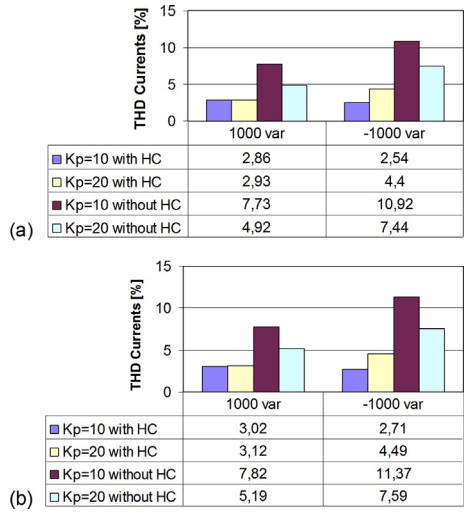

Fig. 32. Comparative analysis between different values of reactive power, with/without HC: (a) Simulation results; (b) Experimental results.

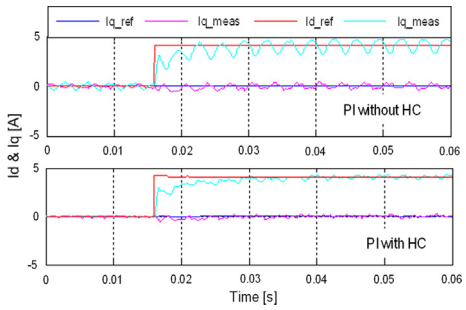

Fig. 33. Reference and measured *dq* current components.

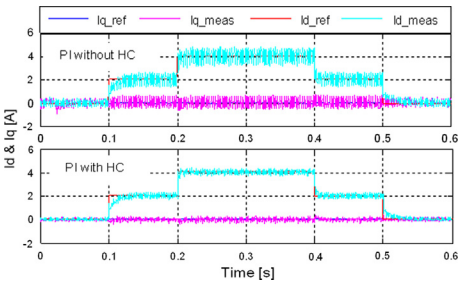

Fig. 35. Reference and measured *dq* current components.

active power reference values without and with HC, while the reactive power reference was set to 0. Based on these results, it can be concluded that the PI controller with HC implemented in *dq* synchronous rotating frame has the best performance for $K_p = 10$, in both simulation (Fig. 31a) and experimental results (Fig. 31b). However, if the HC is not implemented, the $K_p = 20$ case has a smaller THD in both situations.

In Fig. 32, the comparative analysis was made at two different reference values of reactive power (1000 var and −1000 var) without and with HC, while the active power reference was set to 2000 W.

As in the previous case, the best performance is obtained for $K_p = 10$ with HC, for both reactive power references, in both simulations (Fig. 32a) and experimental results (Fig. 32b). Comparing the results obtained for both values (1000 var/−1000 var), it can be seen that a better energy quality is obtained for $Q^* = -1000$ var for $K_p = 10$, in both simulation and experimental cases, with HC. Also, for $Q^* = 1000$ var compared with $Q^* = -1000$, the $K_p = 20$ case has a smaller THD, without and with HC.

3.4. Case 4: step change in the active power reference for PI controller parameters ($K_p = 10$, $K_i = 1000$, $K_{i5,7} = 150$), without and with HC

Fig. 33 shows the reference and measured *dq* current components for a step change in the active current reference (I_{d_ref}) at 0.015 s, while the reactive current reference is maintained constant at $I_{q\_ref} = 0$ A, for the PI current controller, without and with HC. These results confirm that the proposed control algorithm is stable at full-supply voltage, achieves zero steady-state error at fundamental frequency and has a good transient response.

Fig. 34 shows the measured grid currents for a step change in the active current reference at 0.015 s, while the reactive current reference is zero.

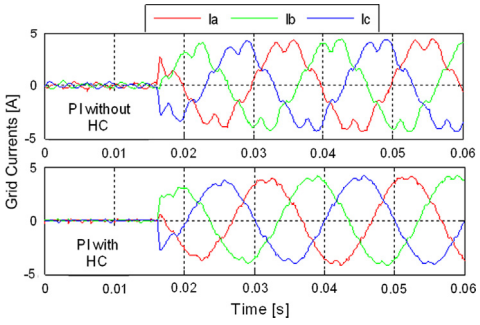

Fig. 34. Measured grid currents waveform for $P_{inv} = 2000$ W and $Q_{inv} = 0$ var.

A good transient behavior of the PI controller can be noticed in this situation. The current is controlled according to its new reference and the output power of the converter smoothly reaches its new operating point.

3.5. Case 5: stairs change in the active power reference for PI controller parameters ($K_p = 10$, $K_i = 1000$, $K_{i5,7} = 150$), without and with HC

In order to test again the transient performance of the controller with adopted software method, a stairs change in the current reference I_{d_ref} was applied (while keeping $I_{q\_ref} = 0$). The reference and measured *d* and *q* axis currents obtained in this case are shown in Fig. 35. The reference for the active power was varied in five steps, each with the width of 100 ms. The stairs were created starting from 0 to 2000 W.

It can be noticed that they closely follow the reference, which means that the current controller is very well tuned. All the active power generated was again injected into the grid via the step-up transformer. The transient response of the measured output currents is shown in Fig. 36; it can be seen that their increase is directly proportional with the active power reference step variation. A zoom in the grid currents is done and the behavior of these currents following the step in power reference can be also seen in Fig. 36. It is easy to notice how the three phase currents are increasing or decreasing according to the reference power changes and as such the results are according to the expectations.

As can be seen in Figs. 31 and 32, there is little difference between the simulation and experimental results. This means that the software method used to estimate the results of PI-based controllers is validated by the experimental measurements with the aforementioned precision. Thus, the adopted simulation method

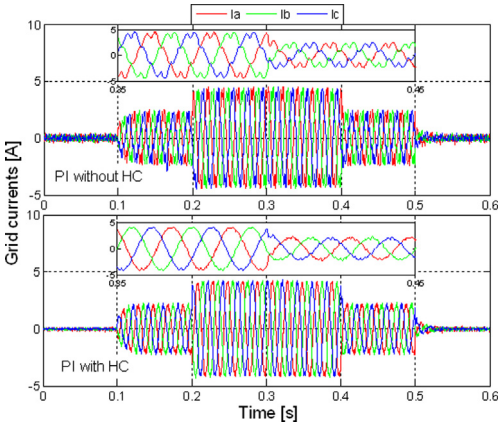

Fig. 36. Measured grid currents waveform for $P_{inv} = 2000$ W and $Q_{inv} = 0$ var.

can successfully be used for design purposes (no further experimental validation being required), reducing the costs and the implementation time.

As reported in all studied cases, these control strategies are performing well under normal and transient grid conditions.

4. Conclusions

In this paper the behavior of interfacing system connecting renewable energy sources to the utility grid by means of a VSI has been presented. A *dq*-PI control strategy has been applied in order to design a current controller for grid-connected VSI, with the main focus on harmonics distortion and tracking performance (see Figs. 12 and 18). As reported in previous works above, these control strategies are performing well under normal and transient grid conditions.

The configuration was modeled and simulated in Matlab/Simulink, implemented in a dSPACE platform and tested with an experimental test setup. Experimental results have been obtained on a 2.2 kVA inverter prototype tested for different operating conditions, including active and reactive power variations and current harmonic compensation. A good current tracking performance of the system in steady state operation and performance in terms of grid current THD was obtained.

A comparison was provided in terms of the harmonic content dependent on the controller structure between the two versions (with and without HC). It can be noticed that, for $\cos\varphi = 1$:

- without harmonics compensation, the system does not comply with the IEEE 1547.2 standard in terms of harmonic content;
- by compensating the 5th and 7th harmonics, the system is within the standards, at rated power and at partial powers representing 75% from the rated one, for $K_p = 10$;
- without HC, a lower harmonic content is achieved in the case of $K_p = 20$.

The comparative analysis presented in Fig. 31 between different proportional controller gains and different active power reference values, has shown a good regulation response in steady state operation, in both simulation and experimental cases. If the reactive power circulation is considered, the THD level decreases. Nevertheless, the HC is required to significantly reduce the harmonic content. The filtering effect of reactive loads is more pronounced for inductive ones.

The reactive power circulation had a good influence on the grid currents harmonic content (Fig. 32) in both cases for both values (1000 var/−1000 var).

Step change in the active power reference and stairs change in the active power reference, shows good controller behavior in the case of a sudden increase/decrease in load. The current is controlled according to its new reference and the output power of the converter smoothly reaches its new operating point.

As can be seen in Figs. 31 and 32, there is little difference between the simulation and experimental results. This means that the results estimation method for PI-based controllers is validated as precise by the experimental measurements.

Thus, the adopted simulation method can be successfully used for design purposes (no further experimental validation being required), reducing the costs and the implementation time.

The simulations validated by the experimental implementation show that the proposed control method (PI current controller with HC and a three-phase DSOGI-PLL) ensures good effectiveness in meeting the stringent grid harmonic standard and is suitable for DPGS applications.

Acknowledgment

The authors wish to thank the Institute of Energy Technology, Aalborg University of Denmark, which, through Professor Remus Teodorescu, gave us the opportunity to experiment the control method, presented in the paper, in their Green Laboratory.

References

[1] Angel Bayod-Rújula A. Future development of the electricity systems with distributed generation. Energy 2009;34:377–83.
[2] Alsayegh O, Alhajraf S, Albusairi H. Grid-connected renewable energy source systems: challenges and proposed management schemes. Energy Convers Manag 2010;51:1690–3.
[3] Carmeli MS, Castelli-Dezza F, Mauri M, Marchegiani G, Rosati D. Control strategies and configurations of hybrid distributed generation systems. Renew Energy 2012;41:294–305.
[4] Kaundinya DP, Balachandra P, Ravindranath NH. Grid-connected versus stand-alone energy systems for decentralized power—a review of literature. Renew Sustain Energy Rev 2009;13:2041–50.
[5] Prodromidis GN, Coutelieris FA. A comparative feasibility study of stand-alone and grid connected RES-based systems in several Greek Islands. Renew Energy 2011;36:1957–63.
[6] Altın M, Göksu Ö, Teodorescu R, Rodriguez P, Jensen BB, Helle L. Overview of recent grid codes for wind power integration. In: Proc IEEE OPTIM 2010. pp. 1152–60.
[7] Kolar JW, Friedli T, Rodriguez J, Wheeler PW. Review of three-phase PWM AC–AC converter topologies. IEEE Trans Ind Electron 2011;58(11):4988–5006.
[8] Melício R, Mendes VMF, Catalão JPS. Comparative study of power converter topologies and control strategies for the harmonic performance of variable-speed wind turbine generator systems. Energy 2011;36:520–9.
[9] Pouresmaeil E, Montesinos-Miracle D, Gomis-Bellmunt O, Bergas-Jané J. A multi-objective control strategy for grid connection of DG (distributed generation) resources. Energy 2010;35:5022–30.
[10] Busada CA, Jorge SG, Leon AE, Solsona JA. Current controller based on reduced order generalized integrators for distributed generation systems. IEEE Trans Ind Electron 2012;59(7):2898–909.
[11] Ramirez D, Martinez S, Carrero C, Platero AC. Improvements in the grid connection of renewable generators with full power converters. Renew Energy 2012;43:90–100.
[12] Bouafia A, Gaubert J-P, Krim F. Design and implementation of predictive current control of three-phase PWM rectifier using space-vector modulation (SVM). Energy Convers Manag 2010;51:2473–81.
[13] Zeng Q, Chang L. Study of advanced current control strategies for three-phase grid-connected PWM inverters for distributed generation. In: Proc IEEE CCA 2005. pp. 1311–6.
[14] Bahrani B, Kenzelmann S, Rufer A. Multivariable-PI-based dq current control of voltage source converters with superior axis decoupling capability. IEEE Trans Ind Electron 2011;58(7):3016–26.
[15] Teodorescu R, Lisserre M, Rodigruez P. Industrial/Ph.D. Course in power electronics for renewable Energy systems, PERES – in theory and practice. Aalborg University; 2010.
[16] Teodorescu R, Blaabjerg F, Borup U, Liserre M. A new control structure for grid-connected LCL PV inverters with zero steady-state error and selective harmonic compensation. In: Proc IEEE APEC 2004. pp. 580–6.
[17] Yuan X, Merk W, Stemmler H, Allmeling J. Stationary-frame generalized integrators for current control of active power filters with zero steady-state error for current harmonics of concern under unbalanced and distorted operating conditions. IEEE Trans Ind Appl 2002;38(2):523–32.
[18] Zmood DN, Holmes DG, Bode GH. Frequency-domain analysis of three-phase linear current regulators. IEEE Trans Ind Appl 2001;37(2):601–10.
[19] Hamrouni N, Jraidi M, Chérif A. New method of current control for LCL-interfaced grid-connected three phase voltage source inverter. Revue des Energies Renouvelables 2010;13(1):1–14.
[20] Blaabjerg F, Teodorescu R, Liserre M, Timbus AV. Overview of control and grid synchronization for distributed power generation systems. IEEE Trans Ind Electron 2006;53(5):1398–409.
[21] Rodriguez P, Teodorescu R, Candela I, Timbus AV, Liserre M, Blaabjerg F. New positive-sequence voltage detector for grid synchronization of power converters under faulty grid conditions. In: Proc IEEE PESC 2006. pp. 129–35.
[22] Zhong QC. Harmonic droop controller to reduce the voltage harmonics of inverters. IEEE Trans Ind Electron 2013;60(3):936–45.
[23] Guerrero JM, Vasquez JC, Matas J, de Vicuna LG, Castilla M. Hierarchical control of droop-controlled AC and DC microgrids – a general approach towards standardization. IEEE Trans Ind Electron 2011;58(1):158–72.
[24] Hatua K, Jain AK, Banerjee D, Ranganathan VT. Active damping of output *LC* filter resonance for vector-controlled VSI-fed AC motor drives. IEEE Trans Ind Electron 2012;59(11):334–42.
[25] Fekete K, Klaic Z, Majdandzic L. Expansion of the residential photovoltaic systems and its harmonic impact on the distribution grid. Renew Energy 2012;43:140–8.
[26] ***IEEE 1547.2-IEEE standard for interconnecting distributed resources with electric power systems; 2008.